Cell Biochemistry and Biophysics (2025) 83:3369–3381
https://doi.org/10.1007/s12013-025-01718-1

ORIGINAL PAPER

Computational Development of Allosteric Peptide Inhibitors Targeting LIM Kinases as a Novel Therapeutic Intervention

Nagarajan Hemavathy[1] · Sampathkumar Ranganathan[2] · Vetrivel Umashankar[3] · Jeyaraman Jeyakanthan[1]

Accepted: 2 March 2025 / Published online: 18 March 2025

Abstract

LIM Kinases (LIMKs) have emerged as critical therapeutic targets in cancer research due to their central role in regulating cytoskeletal dynamics and cell motility via cofilin phosphorylation. Allosteric inhibitors, which bind outside the ATP-binding pocket, offer distinct advantages over ATP-competitive inhibitors, such as increased specificity, reduced off-target effects, and the ability to overcome resistance. This study investigates a series of novel tetrapeptides mimicking the binding mode of TH470, an allosteric LIMK inhibitor, using in silico docking and molecular dynamics simulations to identify potential lead compounds with high specificity, binding affinity, and favorable pharmacokinetic properties. Structural analyses revealed critical interactions between TH470 and LIMKs, particularly with conserved residues such as Thr405 (gatekeeper residue), Ile408 (hinge region), and Asp469 (XDFG motif), which are essential for stabilizing inhibitor binding. Molecular dynamics simulations confirmed the stability of TH470-LIMK1 and TH470-LIMK2 complexes, with lower RMS deviations and robust interaction patterns enhancing binding affinity. From the set of tetrapeptides mimicking TH470 binding mode, only YFYW, WPHW, and YWFP for LIMK1, and PYWG, FYWV, and WFVW for LIMK2 demonstrated high binding affinities, non-toxic profiles, and promising anti-cancer, anti-angiogenic, and anti-inflammatory properties. Among the studied peptides, LIMK1-YFYW and LIMK2-WFVW exhibited the most substantial binding affinities, supported by high hydrogen bond occupancy with key residues such as Ile416 and Thr405. The findings highlight the therapeutic potential of allosteric peptide inhibitors targeting LIMK-mediated pathways in cancer progression. The study underscores the importance of specific interactions with conserved LIMK residues, providing a foundation for further developing selective inhibitors to modulate actin dynamics and combat cancer-related processes.

Keywords Allosteric inhibitors · Peptide · Type –III · LIMKs · Molecular dynamics · MM/PBSA

Introduction

Allosteric inhibitors are small molecules that target kinases by binding to regions other than the enzyme's active site [1]. This noncompetitive binding induces conformational changes, modulating kinase activity by inhibiting or altering the enzyme's function. Unlike traditional ATP-competitive inhibitors, allosteric inhibitors offer enhanced specificity because their binding sites are often less conserved across kinases [2, 3]. This characteristic reduces the likelihood of off-target activity and toxicity while bypassing resistance caused by mutations in the ATP-binding pocket [4]. Notable examples of allosteric inhibitors include trametinib, asciminib, and rapamycin [4, 5].

Allosteric inhibitors are divided into two main categories: inhibitors that bind adjacent to but do not overlap with the ATP site (type III) and those that bind to an allosteric site distal to the ATP site (type IV) [4]. Although type-III and type-IV inhibitors offer potential advantages, they are much rarer than other classes, and only a small number have been FDA-approved [6]. This scarcity is primarily due to challenges in identifying allosteric regulatory sites and determining their mechanisms of action.

Type III inhibitors bind near the ATP-binding pocket in the catalytic domain of the kinase but do not interact with the

✉ Jeyaraman Jeyakanthan
jjbioinformatics@gmail.com

[1] Structural Biology and Bio-Computing Lab, Department of Bioinformatics, Science Block, Alagappa University, Karaikudi, Tamil Nadu, India

[2] Centre for Bioinformatics, KBIRVO, Vision Research Foundation, Chennai, India

[3] Virology & Biotechnology/Bioinformatics Division, ICMR-National Institute for Research in Tuberculosis, Chennai, Tamil Nadu, India

hinge region [7, 8]. These inhibitors include molecules that bind in the hydrophobic pocket formed by the DFG-out conformation. For instance, the TH257 hinge fusion analog TH470 is a promising example [3]. Type III inhibitors show great potential in targeting LIM kinases (LIMKs), which regulate actin cytoskeleton dynamics [9]. By binding to allosteric sites, these inhibitors modulate LIMK activity with high specificity, which can overcome resistance associated with ATP-competitive inhibitors [10]. LIMK inhibition affects processes like cell migration and invasion, making type III inhibitors valuable in cancer treatment, particularly in breast, glioblastoma, and prostate cancer [11, 12].

LIMKs are crucial in various diseases, especially cancer and neurological disorders [13–16]. They regulate actin dynamics by phosphorylating cofilin, thus influencing the cytoskeleton's structure [17, 18]. Dysregulated LIMK activity has been linked to cancer progression, including cell proliferation, migration, and metastasis [8, 19–23]. Beyond cancer, LIMKs are also associated with neurological disorders such as neurofibromatosis, schizophrenia, and Alzheimer's disease [24–28]. Targeting LIMKs with selective inhibitors, especially allosteric inhibitors, offers a promising therapeutic approach for managing oncological and neurological conditions.

Peptide inhibitors mimicking type III kinase inhibitors bind to regulatory regions outside the ATP-binding pocket [29–32]. Stabilizing the kinase in its inactive form prevents ATP or substrate binding [33]. These peptide inhibitors can achieve higher specificity by binding to less conserved kinase regions. They can also be designed to target protein-protein interactions, making them powerful tools in cancer therapy [32, 34–36]. However, peptide inhibitors have not yet been explored as a therapeutic agent for LIMKs. Therefore, using structural bioinformatics approaches, this study investigated tetrapeptide mimicking TH470 binding mode in both LIMK1 and LIMK2.

Methodology

Structure Preparation and Molecular Dynamics Simulation Analysis

The crystal structures of the inactive state [DFG_{out} αC_{out}] (CODO) of LIMKs, in complex with the Type-III inhibitor TH470, were retrieved. These include PDB IDs 7B8W (LIMK1-TH470) [37] and 7QHG (LIMK2-TH470) [38]. The structures were then remodeled using Modeller 9.24 to fix missing residues and atoms [39]. Among the generated models, the one with the least DOPE score was selected as the best model. Subsequently, the remodeled structures were preprocessed and refined using the Protein Preparation Wizard module in the Schrodinger suite [40]. Prior to the MD simulation, the redocking was performed for the co-crystallized LIMKs-TH470 complexes using AutoDock Vina [41]. Further MD simulation was carried out using the GROMACS 2022 version [42]. The protein topologies were generated with the CHARMM36M force field, while the topologies for the TH470 ligand were generated using the CGenFF server. The protein-ligand systems were solvated using the spc216 water model and neutralized with counter ions. The Energy minimization was performed using the steepest descent algorithm, followed by equilibration in the NVT and NPT ensembles to stabilize the system's temperature of 315 K and a pressure of 1 bar. The production run was then carried out under periodic boundary conditions for 200 ns at 315 K. The simulation trajectory was finally analyzed to evaluate the structural stability, protein-ligand interaction, and conformational dynamics through RMSD, RMSF, and H-bond analysis with secondary structural changes using GROMACS utilities.

Prioritisation of Tetrapeptide Inhibitors Targeting LIMKs

In this study phase, virtual screening of tetrapeptides against inactive LIMK1 and LIMK2 structures was performed using the PepVis pipeline [43], as described in our previous study (to be published), based on a grid generated over the TH470 interacting residues. The top 20 peptides with the highest Vina scores were shortlisted for further evaluation. Using the CSM-peptide analysis server [44], the peptides were first assessed for their anti-cancer, anti-angiogenic, and anti-inflammatory properties. Only those peptides with scores above the threshold of 0.5 were considered for the next step. These peptides were then subjected to toxicity analysis using the ToxIBTL [45] and ToxinPred 3.0 [46] servers. Based on consensus results from both toxicity servers, only the non-toxic peptides were advanced to the interaction profiling analysis stage. Subsequently, the PLIP server [47] evaluated the non-toxic peptides with favorable anti-cancer and anti-angiogenic properties for interaction profiling. Peptides showing interactions similar to the reference inhibitor TH470 were selected for binding free energy calculations via the HawkDock server [48]. This allowed for a detailed understanding of the energy components contributing to the stability of the peptide-LIMK complexes. In addition, the physiochemical properties of the shortlisted peptides were processed using https://pepcalc.com/. Finally, MD simulation was performed to assess the structural stability of these complexes.

MD Simulation and Binding Energy Analysis

MD simulation for protein-peptide complexes for 200 ns was carried out using the GROMACS 2022 package,

following the protocol of LIMK1/2 with their type III inhibitor, as discussed in the section above. The gmx_MMPBSA tool evaluated the interaction between the LIMK1/2 with its inhibitor and screened peptides based on the MD simulations for binding free energy calculations [49–52]. Further, 500 frames were sampled from the last 100 ns of the simulation trajectory for this analysis. Furthermore, the binding free energy ΔG bind was computed using the following equation:

$$\Delta Gbind = \Delta EMM + \Delta Gsolv - T\Delta S$$

ΔE_{MM} represents the molecular mechanics energy, consisting of van der Waals and electrostatic energy interactions. ΔG_{solv} denotes the solvation-free energy, combining both polar and non-polar contributions. Whereas the $-T\Delta S$ accounts for the entropy of the simulation system. The total binding energy was determined by averaging the energy components across all 500 simulation frames and tabulated.

Results and Discussion

Structure Preparation and Molecular Dynamics Simulation Analysis

The interaction profiling of TH470 in complex with LIMK1, as shown in Fig. 1a, infers that TH470 forms a hydrogen bond with the Gatekeeper (GK) residue, Thr413 and Asp478 of XDFG segment, followed by 2 hydrogen bonds with the hinge residue, Ile416. Besides the hydrogen bond, the hydrophobic interactions were observed to be maintained with the conserved kinase residues, namely, βIII (Lys368, Leu370), b.L (Val396, Leu397), βV (Phe411), GK (Thr413), Hinge (Thr415), αE (Leu451), βVII (Leu467), βVIII (Val476), XDFG (D478), a.l (Leu481). In LIMK2-TH470 (Fig. 1b), hydrogen bonds with GK (Thr405), Asp469, and two H-bonds with Hinge (Ile408), followed by π-cation with βIII (Lys360). Apart from these interactions, hydrophobic interactions were also formed with conserved kinase residues, namely, βIII (Lys360), b.L (Val388, Leu389), βV (Leu403), GK (Thr405), αE (Leu442), XDFG (D469), a.l (Leu472, Arg474). The interaction analysis of the TH470 with LIMK's showed that the 2-aminothiazole moiety acts as a hinge-binder and the phenylsulfamoyl moiety in the DFG-out pocket (Fig. 1). Moreover, the redocking of the co-crystallized TH470 showed a Vina score of −8.054 (kcal/mol) and −6.711 (kcal/mol) with LIMK1 and LIMK2 respectively. (Supplementary Table S1).

The LIMK1-TH470 complex was initially observed to have RMS deviations of ~0.42 nm for ~50 ns (Fig. 2a). Yet, the system has tended to be well equilibrated after ~50 ns with an RMSD of ~0.38 nm and maintained throughout the MD run, indicating the stability of the complex. The RMSD analysis of the LIMK2-TH-470 complex reveals that despite initial higher RMS deviations, after ~65 ns, the system has tended to equilibrate and stabilize with the RMS deviation of ~0.38 nm (Fig. 2d). The RMSF profiling of LIMK1 showed that higher fluctuations were attained by the 493–504 residues (extended a.l segment spanning the loop conformation) with RMSF values ranging from 0.46–0.54 nm followed by residue 526 (~ 0.38 nm) (Fig. 2b). In the case of LIMK2, the 485–494 segment (extended a.l segment spanning the loop conformation) fluctuated with

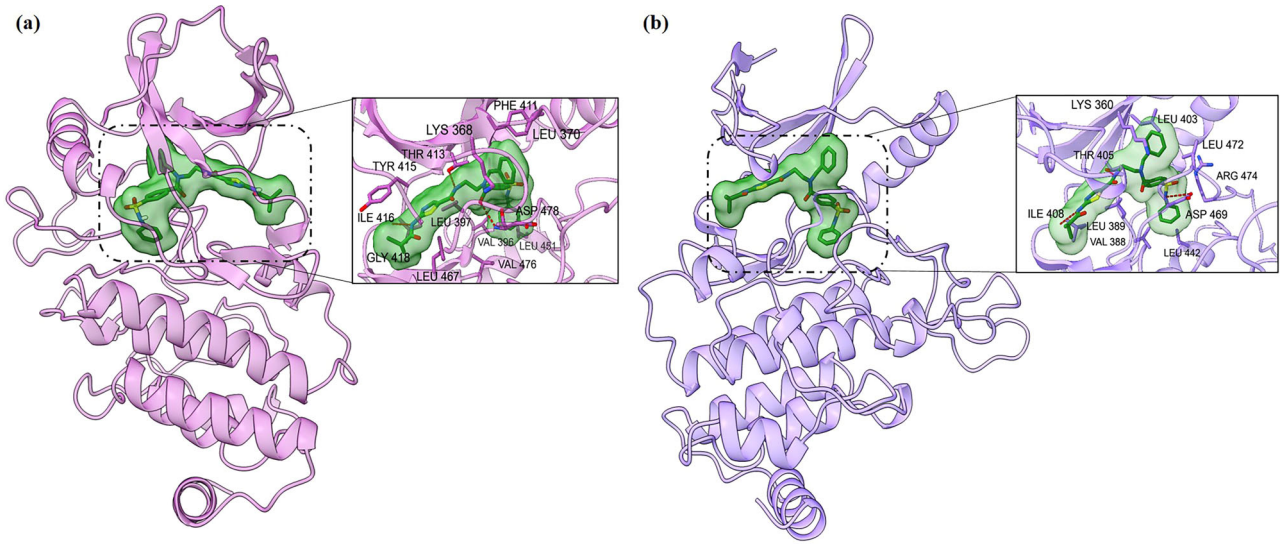

Fig. 1 Three-dimensional structure of refined LIMK1 and LIMK2 complexes with TH470 (**a**) Interaction of LIMK1 with TH470 and (**b**) Interaction of LIMK2 with TH470

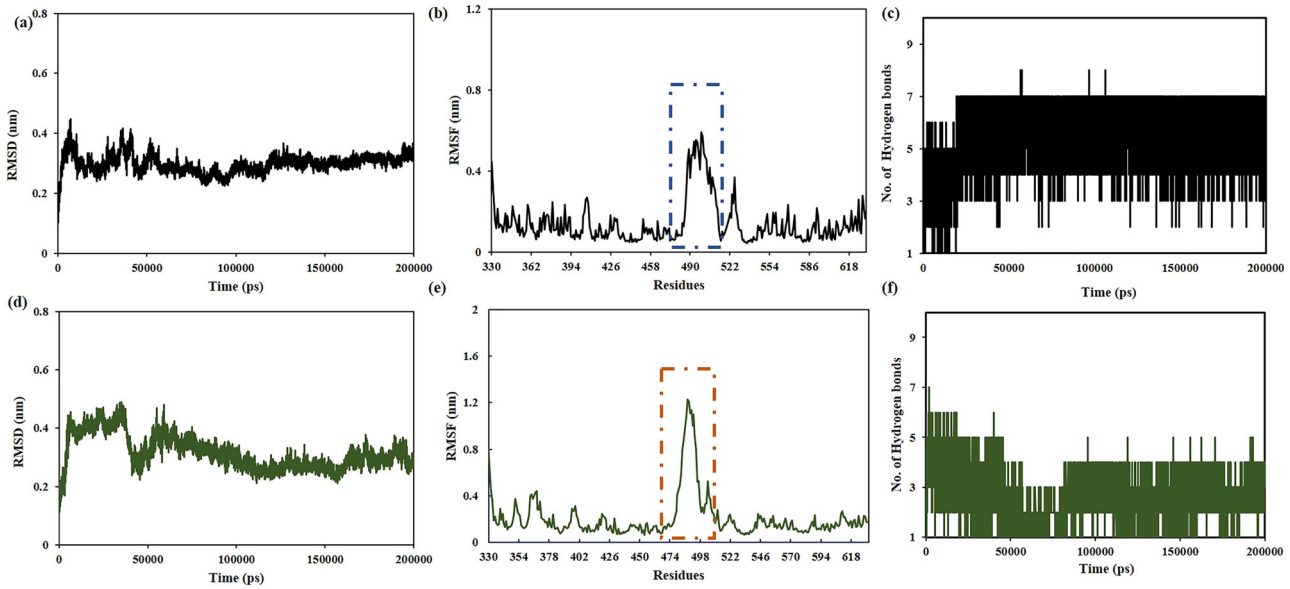

Fig. 2 Molecular dynamics simulation analysis of LIMKs-TH470 complexes; RMSD plot of (**a**) LIMK1-TH470 complex (**d**) LIMK2-TH470 complex; RMSF plot of (**b**) LIMK1-TH470 complex (**e**) LIMK2-TH470 complex; Inter-hydrogen bond analysis of (**c**) LIMK1-TH470 complex (**f**) LIMK2-TH470 complex

RMSF value of ~0.88–1.13 nm (Fig. 2e). As per inter-hydrogen bond analysis, the TH-470 was observed to have maintained ~7 H-bonds and ~4 H-bonds with LIMK1 and LIMK2, respectively (Fig. 2c, f). The PCA and FEL analysis of LIMK-TH470 complexes revealed a single near-native cluster, indicating stable conformations (Supplementary Fig. S1a, b). Interaction analysis of the LIMK1-TH470 complex (Supplementary Fig. S1c), showed hydrophobic interactions with Lys368, Leu397, Thr413, Thr420, Leu451, Leu467, Asp478, Leu481, and Arg483, while hydrogen bonds involved Leu397, Phe399, Ile416, Asp478, and Arg483 (Supplementary Fig. S1e). For the LIMK2-TH470 complex (Supplementary Fig. S1d), hydrophobic interactions were conferred by Lys360, Leu362, Leu403, Thr405, Leu442, Ile447, Asp469, and Arg474, with hydrogen bonds observed at Thr405, Ile408, and Asp469 (Supplementary Fig. S1f).

Selection of Peptide Inhibitors

The tetrapeptides were observed to have docking scores ranging from −9.4–−11.5 kcal/mol with LIMK1 (Supplementary Table S2); however, with LIMK2, the docking scores ranged from −10.4–−11.0 kcal/mol (Supplementary Table S3). Compared to the known inhibitor (TH470), the peptides have shown a higher vina score, indicating that the screened peptides have better binding affinity than TH470. Amongst the top 20 tetrapeptides docked to LIMK1, only 9 tetrapeptides, namely, YPPW, WPRW, PWAP, YWFP, FPRW, RWFP, YFYW, RWPW, WPHW, were predicted to have an anti-angiogenic effect (Fig. 3a). Moreover, except for PWAP, the remaining 8 tetrapeptides' were expected to have anti-cancer properties. Among these 8 tetrapeptides, only YPPW lacked anti-inflammatory properties. Finally, the following tetrapeptides, YWFP, FPRW, YFYW, RWPW, and WPHW, were found to possess anti-angiogenic, anti-cancer, and anti-inflammatory properties and were also observed to be non-toxic (Supplementary Table S4). From the interactions profiling, it was inferred that despite the hydrophobic interaction of Lys368 with all the tetrapeptides, only YFYW, YWFP, and WPHW were observed to form a hydrogen bond with Hinge residue, Ile416, and hydrophobic interaction with Asp478 as that of TH470 (Fig. 4a). Henceforth, only YFYW, YWFP, and WPHW in complex with LIMK1 (Fig. 5a,c–e, Supplementary Fig. S2) were considered for physicochemical property analysis (Supplementary Table S6) and binding free energy analysis. The Electrostatic energy was observed to be highly favored in LIMK1-WPHW, followed by Van der Waals energy in all the complexes. The LIMK1-tetrapeptide complexes were also observed to have binding energy in increasing order as follows: YFYW < WPHW < YWFP with the total binding energy of −54.79 < −64.8 < −66.88 kcal/mol (Supplementary Fig. S3a).

Of the top 20 peptides of LIMK2, 13 were observed to lack anti-angiogenic properties (Fig. 3b). In comparison, the other 7 peptides, namely, YFWA, NWWT, PFWG, PYWG, WWSY, FYWV, and WFVW, featured anti-angiogenic, anti-cancer, and anti-inflammation properties with higher confidence (Fig. 3b). However, amongst these 7 peptides, only 4 were predicted to be non-toxic, while the other three peptides, NWWT, PFWG, and WWSY, were deemed toxic (Supplementary Table S5). Interaction profiling was

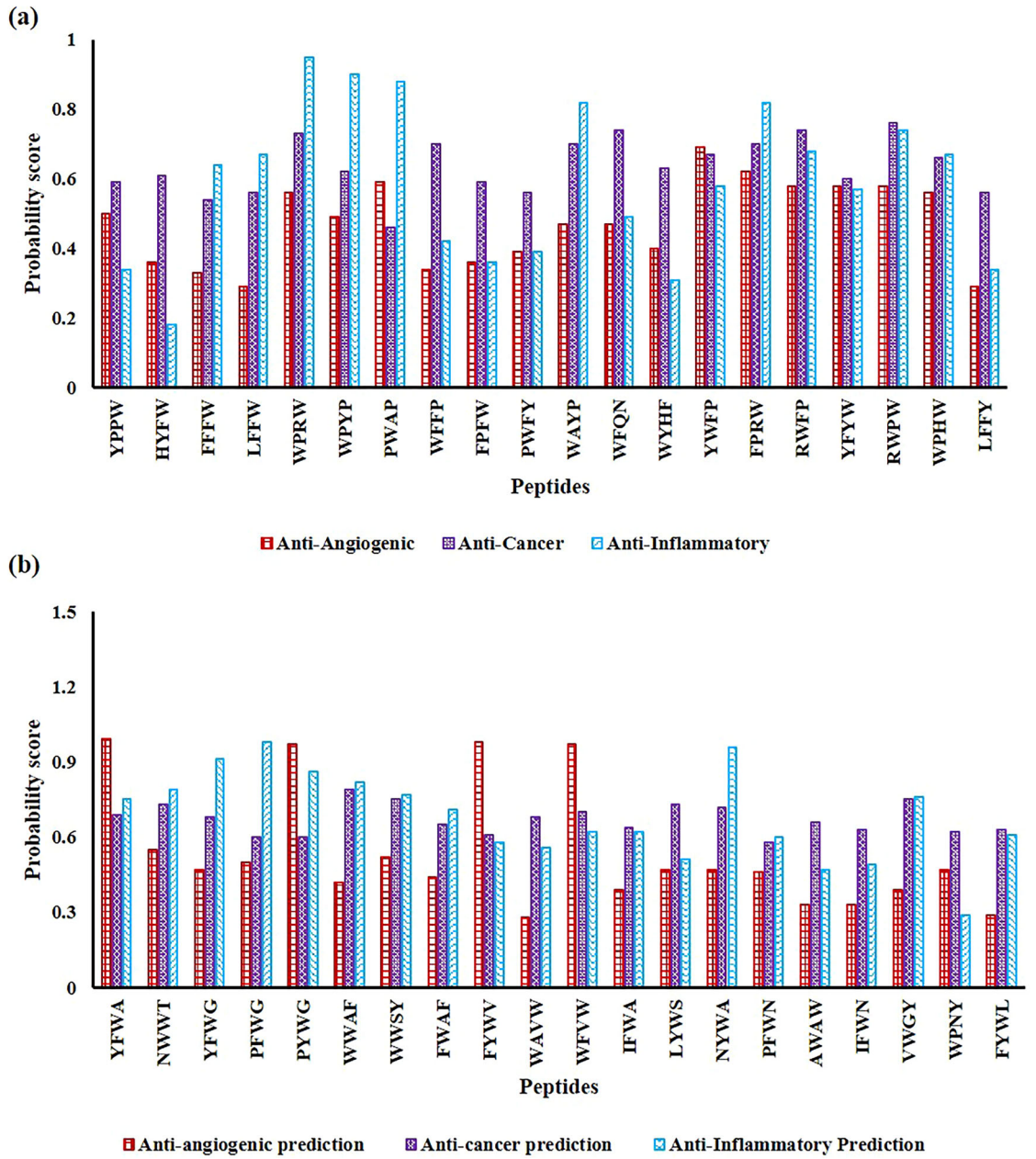

Fig. 3 Property analysis of the top 20 peptides (**a**) LIMK1 (**b**) LIMK2

processed only for the YFWA, PYWG, FYWV, and WFVW peptides in complex with LIMK2 (Fig. 4b). Despite the π-cation interaction and hydrophobic interactions of Lys360, in all the peptides as that of TH470, only PYWG, FYWV, and WFVW were observed to have hydrogen bond with Ile408, the hinge residue similar to TH470 (Fig. 4b). Therefore, only PYWG, FYWV, and WFVW peptides in complex with LIMK2 (Fig. 5b,f–h, Supplementary Fig. S2) were analyzed for their physicochemical properties (Supplementary Table S6) and binding free energy calculations. It was inferred that the electrostatic energy has highly favored the binding affinity of FYWV to LIMK2. However, a higher binding affinity was also observed in the LIMK2-WFVW complex with a binding energy of −70.25 kcal/mol and a higher Van der Waals energy of −90.93 kcal/mol. On the contrary, in the case of the other complexes, the binding affinity was observed to be −62.55 kcal/mol and −44.67 kcal/mol for FYWV and PYWG, respectively (Supplementary Fig. S3b).

Comparative Molecular Dynamics Simulation

The comparative RMSD analysis of LIMK1-tetrapeptide complexes showed that all complexes have maintained well-

(a)

Peptide	β1	g.l					βII	βIII				αC	b.L			βIV	βV	GK	Hinge		Linker	αE	βVII	βVIII	XDFG		a.l
	345LEU	347LYS	348GLY	349CYS	350PHE	351GLY	353ALA	366VAL	368LYS		369GLU	370LEU	383MET	391LEU	396VAL	397LEU	399PHE	411PHE	413THR	414GLU	416ILE	418GLY	451LEU	467LEU	476VAL	478ASP	479PHE	481LEU
FPRW	1		1	2			1	1	1	1				1	1		1	1	1		1						1	1	1
YFYW	2	1					1		2			1		1	1	2		1			2		1			2	1	2	1	1
RWPW	1						1		1	1	1					1				1	2	1		2			2	2	
WPHW	1								1	1				1	1				1		1		1	1		1	2	2	1
YWFP	1				1			2	2	2	1		1	1	1	1	1				2		1	1	1	1	1	2	2

Hydrophobic Interactions
Salt bridges
Hydrogen bond
π-cation
π-Stacking

(b)

Peptide	β1	g.l	βII	βIII				αC	b.L		βIV	βV	GK	Hinge			Linker	αE	βVI	βVII	XDFG		a.l	
	337LEU	342PHE	344GLN	345ALA	358VAL	360LYS		362LEU	373PHE	383LEU	389LEU	391PHE	403LEU	405THR	406GLU	407TYR	408ILE	412THR	442LEU	447ILE	458LEU	469ASP	470PHE	472LEU	474ARG
YFWA	1			1		2	1	2			2	1	2	1	1	1			1		2	1		2	1
PYWG	2					2	1				2		1	1	1	1	1				2	1			
FYWV	2		1	1	1	2	1	1	1	1	1	1	1	1	1	1	1		1		2	1	2	1	1
WFVW	1	1		1		2	1			1			2		2		1	1	2	1	2	1	1	3		1	1

Fig. 4 Interaction profiling of the shortlisted peptide complex with LIMKs (**a**) LIMK1 (**b**) LIMK2

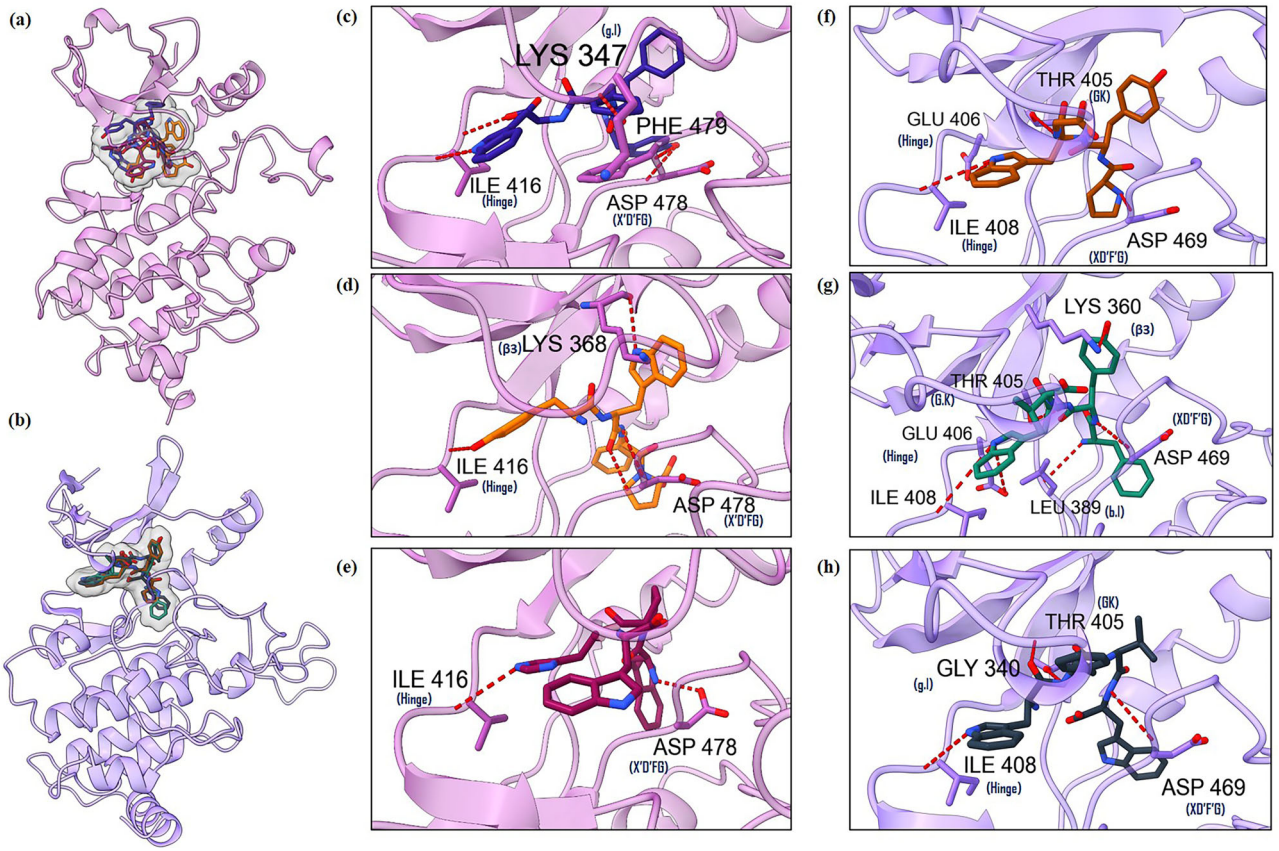

Fig. 5 Three-dimensional structure of LIMK's inhibitor complexes (**a**) LIMK1-TP complex (**b**) LIMK2-TP complex; (**c**) LIMK1-YFYW (**d**) LIMK1-YWFP (**e**) LIMK1-WPHW (**f**) LIMK2- PYWG (**g**) LIMK2- FYWV (**h**) LIMK2- WFVW

equilibrated RMS deviations with an RMSD value ranging from ~0.34–0.38 nm (Fig. 6a). Except for the LIMK1-YWFP complex, which has shown higher RMS deviations in the last ~40 ns with an RMSD value of ~0.47–0.53 nm, other complexes have maintained the least RMSD deviations and stabilized throughout the MD production run (Fig. 6a). Of the LIMK2-tetrapeptide complexes, only LIMK2-FYWV complex has shown higher RMS deviation of ~0.58–0.76 nm after

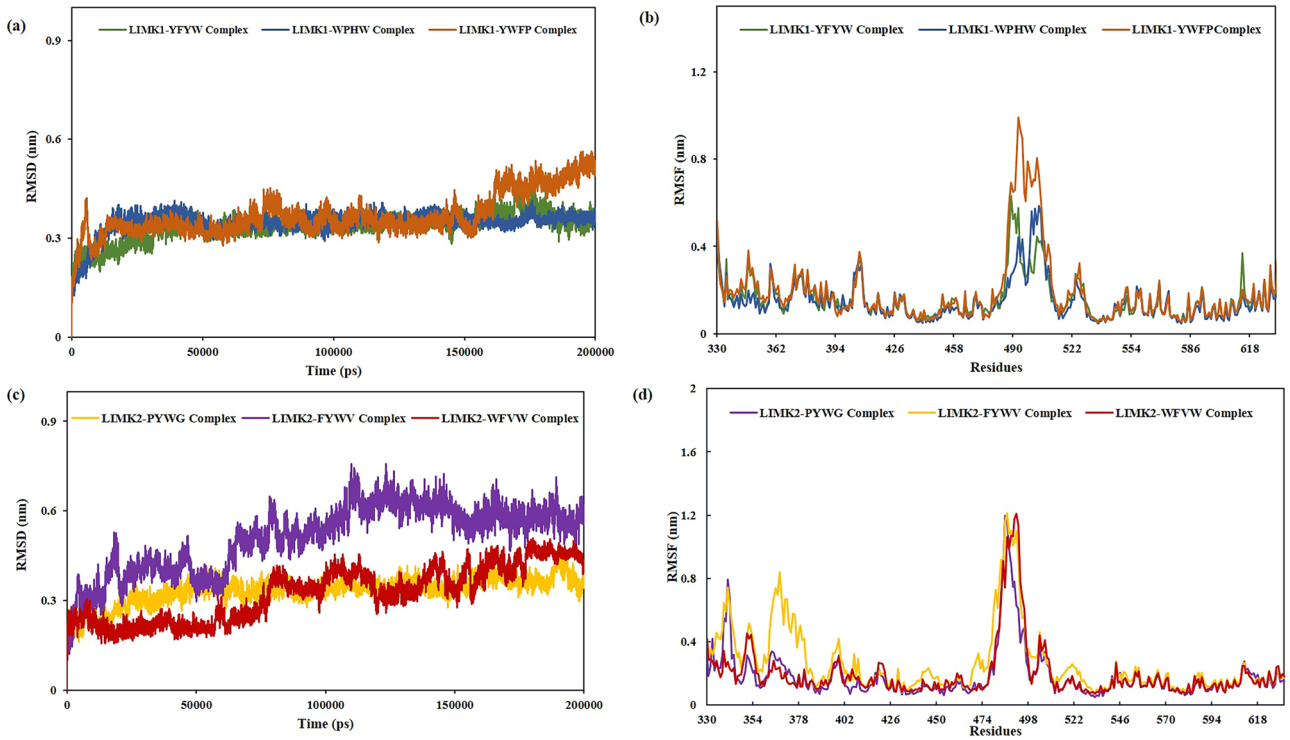

Fig. 6 Molecular dynamics simulation analysis of LIMKs-peptide complexes; Comparative RMSD plot of (**a**) LIMK1-peptide complexes (**c**) LIMK2- peptide complexes; Comparative RMSF plot of (**b**) LIMK1-peptide complexes (**d**) LIMK2- peptide complexes

~57 ns, yet has tried to equilibrate in the last ~50 ns of MD run (Fig. 6c). At the same time, the other LIMK2-tetrapeptide complexes have maintained RMS deviations of ~0.36 nm and were observed to be well equilibrated till the end of the MD production run (Fig. 6c). When compared to the TH470 in complex with LIMK1 and LIMK2, except for LIMK1-YWFP complex and LIMK2-FYWV complex, all the other complexes have featured the least deviations (Supplementary Fig. S4a, b).

Regarding the comparative RMSF profiling (Fig. 6b, d), the a.l segment has fluctuated highly in both LIMK1 and LIMK2 in complex with tetrapeptides. With respect to the a.l segment in LIMK1, the LIMK1-YWFP complex has attained higher fluctuations ~1.1 nm, followed by LIMK1-YFYW complex and LIMK1-WPHW complex (Fig. 6b). Amongst the LIMK2-tetrapeptide complexes (Fig. 6d), except for the LIMK2-FYWV complex, which has shown higher fluctuations at the N-lobe kinase domain residues, specifically, Glu368 with RMSF value of 0.856 nm, all the complexes have highly fluctuated specifically at the a.l segment, to be specific the Lys487-Lys492 loop conforming residues showed RMSF values ranging 1.08–1.21 nm. The comparative RMSF analysis of TH470 with LIMK1 and LIMK2 (Supplementary Fig. S4c, d) also indicates that except for the LIMK1-YWFP complex, all the peptide complexes have shown similar RMSF profiling.

On analyzing the RMSD profiling of the peptides (Supplementary Fig. S5), it was inferred that the peptides had shown fewer RMS deviations than the LIMK1 and LIMK2, with RMSD values ranging from ~0.05−0.12 nm and ~0.04–0.2 nm. Of all the LIMK1-tetrapeptide complexes, the YFYW peptide has shown a higher RMS deviation of ~0.14 nm than other peptides (Supplementary Fig. S5a). Except for the last ~70 ns of higher deviations up to ~0.2 nm observed in FYWV, all peptides were found to have maintained the least stable RMS deviations throughput MD run (Supplementary Fig. S5b). Despite high RMSF values of ~0.18 nm and ~0.25 nm, the YFYW and FYWV peptides were in complex with LIMK1 and LIMK2, respectively, and all the peptides have featured the least RMS fluctuations (Supplementary Fig. S5c, d).

The comparative inter-Hbond analysis of the LIMK's tetrapeptide complexes shows that the LIMK1-YFYW complex has shown nearly 7 H-bonds till ~82 ns, while the LIMK1-YWFP complex has attained 7 H-bonds in the last ~30 ns of MD run (Fig. 7a). However, on average, all the LIMK1- tetrapeptide complexes were found to have maintained ~6 H-bonds throughout the MD simulation, increasing the complexes' stability (Fig. 7a). Moreover, the hydrogen bond occupancy analysis of the complexes reveals that the H-bond occupancy of hinge residue Ile416 is to have been maintained highly in the LIMK1-TH470 complex, followed by the LIMK1-WPHW complex. Of all the conserved kinase domain residues, the GK residue Thr413 has maintained H-bond occupancy ranging from

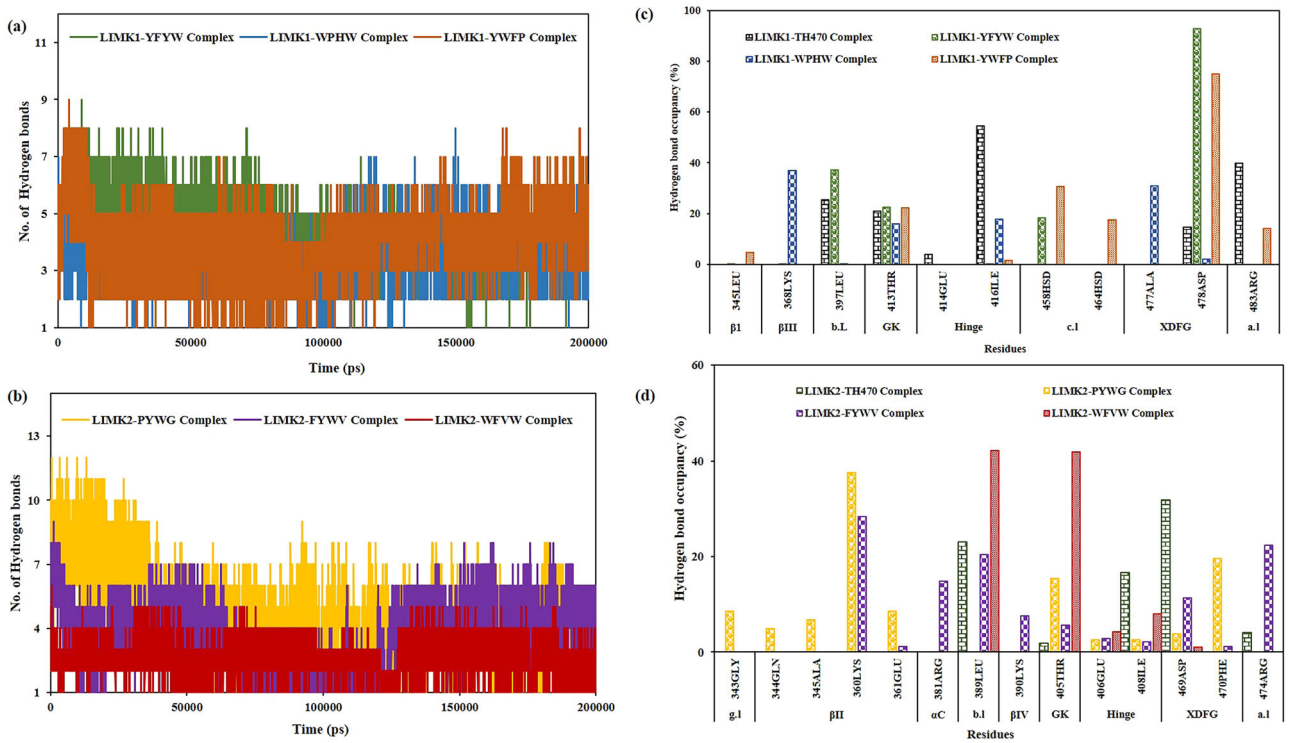

Fig. 7 Comparative inter-hydrogen bond analysis of LIMKs with tetrapeptides and TH470 (**a**) LIMK1-inhibitor complexes (**b**) LIMK2-inhibitor complexes; Comparative H-bond occupancy plot of (**c**) LIMK1-inhibitor complexes (**d**) LIMK2- inhibitor complexes

15.99–22.54% in all the LIMK1 complexes (Fig. 7c). In comparison, the LIMK1-WPHW complex was the only one that maintained H-bond occupancy with Lys368 (βIII), 477Ala (XDFG motif). Meanwhile, the b.L residue, 397Leu, has maintained an H-bond only in LIMK1-TH470 and LIMK1-YFYW complexes. In addition to the 453Arg (a.l) residue, both the C.l residues have maintained H-bond occupancy in the LIMK1-YWFP complex, apart from the LIMK1-YWFP complex, which showed H-bond occupancy of 30.62 and 17.66% with 458Hsd and 464Hsd of c.l, respectively. Only 458Hsd was observed to have 18.41% H-bond occupancy in the LIMK1-YFYW complex. In comparison, the LIMK1-TH470 complex and LIMK1-YWFP complex had occupancy of 39.97 and 14.14% with Arg483 of a.l (Fig. 7c).

Amongst the LIMK2-tetrapeptide complexes, only the LIMK2-PYWG complex has shown increased H-bonds of nearly 12–10 H-bonds for an initial ~45 ns (Fig. 7b). Yet, the complex has tended to maintain ~7 H-bonds on average throughout the simulation duration, followed by the LIMK2-FYVW complex with increased H-bonds (~6–7 H-bonds) in the last ~70 ns of the MD run. The LIMK2-WFVW complex was observed to have fewer H-bonds than other complexes and has tried to manage nearly 4 H-bonds on average throughout MD (Fig. 7b). The LIMK2-PYWG complex has maintained a higher degree of occupancy with most conserved kinase domain residues, followed by the LIMK2-FYWV complex (Fig. 7d). The hinge residue, Ile408, had higher H-bond occupancy of 16.67 and 7.96% in the LIMK2-TH470 and LIMK2-WFVW complex, respectively, while negligible occupancy was observed in other complexes. LIMK2-WFVW is the only complex that has maintained higher occupancy with both Leu389 (b.l) and Thr405 (GK) of 42.1 and 41.85%, respectively. In terms of βII, the complex LIMK2-PYWG has maintained an occupancy with most of the residues, namely, Gln344, Ala345, Lys360, and Glu361, along with Thr405 (GK), wherein the Lys360 was observed to have occupancy with LIMK2-FYWV complex too with an occupancy of 28.29%. Other than Lys360, the LIMK2-FYWV complex had occupancy with Arg381 (αC) [14.8%], Leu389 (b.l) [20.42%], Lys390 (βIV) [7.59%], Thr405 (GK) [5.66%], Asp469 (XDFG) [11.35%] and Arg474 (a.l) [22.36%] (Fig. 7d).

From the PCA and FEL analysis of the LIMK-peptide complexes (Supplementary Fig. S6, Supplementary Fig. S8), except for the LIMK1-WPHW complex, all the other LIMK-peptide complexes have shown a single near-native cluster, which infers the stability of the complexes. The interaction profiling of LIMK1-YFYW complex inferred hydrophobic interactions with Leu345 (βI), Ala353 (βII), Val385 (αC), Phe399 (βIV), Phe411 (βV), Leu467 (βVII), and Asp478 ("D" FG). In addition, hydrogen bond interactions with Gly346 (g.l), Thr413 (GK), and Asp478 (3)

("D" FG) were observed as shown in Supplementary Fig. S7a. At the same time, the LIMK1-WPHW complex has maintained the hydrophobic interactions with Lys347 (g.l), Val366 (βIII), Lys368 (βIII), Leu391 (b.l), Leu397 (b.l), Thr413 (GK), Asp478 ("D" FG), Phe479 (2) ("D" F" G) along with hydrogen bond interactions with Leu397 (b.l), Ile416 (Hinge), salt bridge interactions with Lys368 (βIII) (Supplementary Fig. S7b). The LIMK1-YWFP has maintained hydrophobic interactions with Lys368 (βIII), Leu391 (b.l), Leu397 (b.l), Leu451 (αE), Leu467 (2) (βVII), Phe479 (D" F" G), Leu481 (a.l) and hydrogen bond interactions with Asp478 ("D" FG) (Supplementary Fig. S7c). At the same time, the LIMK2-PYWG complex showed hydrophobic interactions with Leu337 (βI), Val358 (βIII), Lys360 (βIII), Phe391 (βIV), Leu403 (2) (βV), Tyr407 (Hinge), Leu458 (βVII), Phe470 ("D" FG). Followed by hydrogen bonds with LIMK2 residues, namely, Ile363, Thr405 (GK), Asp469 (2) ("D" FG), and Phe470 (D" F" G), wherein Lys360 (βIII) was observed to form both π-cation and salt bridge interaction with the peptide (Supplementary Fig. S9a). In terms of the LIMK2-FYWV complex, the hydrophobic interactions were maintained with Ala345 (βII), Leu383 (b.l), Thr405 (GK), Leu442 (αE), Ile447 (βVI), Asp469 ("D" FG), and Phe470 (D "F" G). Despite hydrophobic interactions, hydrogen bonds were formed with Leu389, Asp469, and Phe470 (D "F" G) of LIMK2. In addition, a π-stacking with Phe373 (αC) and salt bridge formation with Lys360 (βIII) were formed with the peptide (Supplementary Fig. S9b). LIMK2-WFVW complex hydrophobic interactions Leu337 (2) (βI), Phe342 (g.l), Ala345 (βII), Lys360 (βIII), Leu458 (βVII), Ala468 ("X" DFG), Phe470 (D" F" G), Leu472 (a.l), Hydrogen bonds with Thr405 (GK), Ile408 (Hinge), π-stacking with Phe391 (βIV) (Supplementary Fig. S9c).

Overall, the PCA and FEL analysis revealed that all LIMK-peptide complexes, except LIMK1-WPHW, exhibited a single near-native cluster, indicating their structural stability. The LIMK1-WPHW complex showed multiple clusters, suggesting a more dynamic behavior and less stability than the other complexes. LIMK1-YFYW emerged as the most stable due to its well-defined interactions, particularly with Thr413 and Asp478, forming multiple hydrogen bonds. LIMK1-WPHW exhibited more dynamic behavior due to its salt bridge with Lys368 and fewer stable hydrogen bonds. LIMK2-PYWG demonstrated a robust network of interactions, with hydrophobic contributions and critical salt bridges from Lys360, making it a highly stable complex. LIMK2-FYWV and LIMK2-WFVW showed enhanced binding through π-stacking and salt bridge interactions, which are crucial for maintaining their structural integrity. LIMK1-YFYW and LIMK2-PYWG stand out as the most stable complexes, offering promising insights for selective inhibitor design. The role of residues like Asp478 (LIMK1) and Lys360 (LIMK2) as critical interaction hubs underscores their importance in modulating binding affinity.

Binding Free Energy Analysis of the LIMK's-Inhibitor Complexes

To understand the biophysical basis of molecular recognition of the peptide inhibitors to LIMK's, all the individual contributions to the total binding free energy were calculated for all complexes using the molecular mechanics Poisson−Boltzmann surface area (MM-PBSA) scheme. Figure 8a shows that the G_{GAS} followed by the van der Waals interactions have favored the binding of peptides to LIMK's. On the contrary, the Polar solvation energy and the E_{Surf} mainly disfavor the complex formation Fig. 8a. The

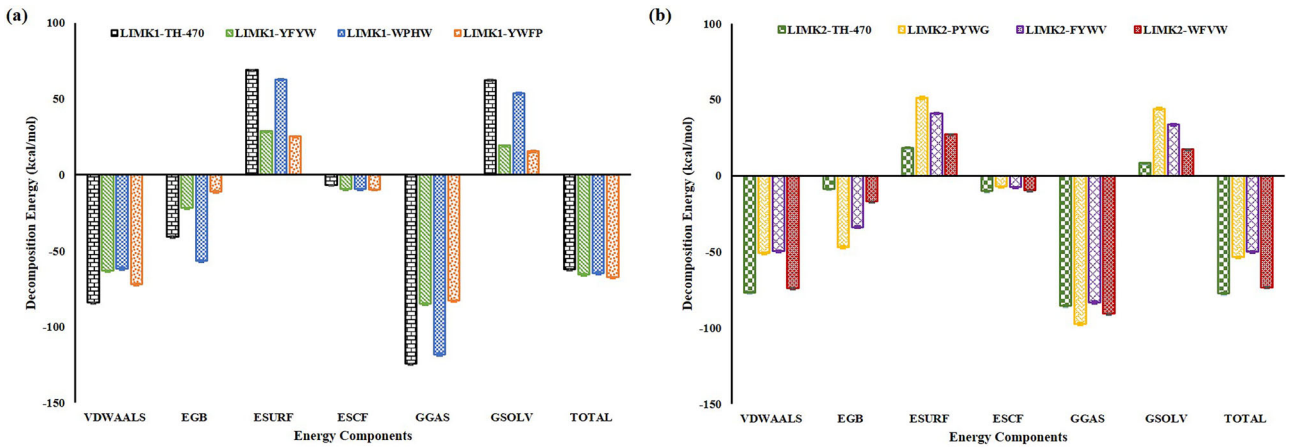

Fig. 8 Represents the summary of the contributions of the peptide inhibitors' binding interactions with the LIMKs, (**a**) LIMK1-tetrapeptide complexes (**b**) LIMK2- tetrapeptide complexes; the energy components described on the x-axis are VDWAALS van der waals energy, EGB generalized born electrostatic solvation energy, ESURF electrostatic surface potential calculation, ESCF electrostatic interaction between the ligand and protein, accounting for the solvent environment using the Generalized Born model, GGAS refers to the gas-phase free energy of the system GB (generalized born), GSOLV refers to calculating solvation effects, particularly polar solvation

total binding energy of the LIMK1-peptide complexes was observed to be in an increased binding affinity as follows: LIMK1-YWFP > LIMK1-YFYW > LIMK1-WPHW >LIMK1-TH470. Overall results showed that the slightly higher binding affinity for LIMK1-peptide complexes compared to LIMK-TH470 complex is due to lesser contributions from the disfavorable components of the binding free energy, such as polar solvation energy. On analyzing the LIMK2-inhibitor complexes (Fig. 8b), the overall sum of G_{GAS} and Esurf show positive results, depicting that the van der Waals interaction is highly dominant in complex formations. Amongst the LIMK2-peptide complexes, only the LIMK2-WFVW complex has shown higher binding affinity with the binding energy of −73.26 kcal/mol in close proximity to that of LIMK2-TH470 (−77.37 kcal/mol) than the other peptides complexes which showed the binding energy of −53.35 kcal/mol (LIMK2-PYWG complex) and −49.83 (LIMK2-FYWV complex) Fig. 8b. In addition, the entropic contribution of the LIMK1-inhibitor complexes (Supplementary Fig. S12a) was inferred that LIMK1-YFYW and LIMK1-YWFP complexes have showed lower entropic contributions, which aids to the higher binding affinity than the reference inhibitor TH470 in complex with LIMK1. Regarding the LIMK2-inhibitor complexes (Supplementary Fig. S12b), only the LIMK2-WFVW complex was observed to have lower entropic contributions than the LIMK2-TH470 complex. The lower entropic contributions observed in these complexes indicate that these peptides (YFYW, YWFP, and WFVW) may attribute to the stable interactions with the respective LIMKs throughout the MD simulation.

Subsequently, the decomposition free energy of individual residues for all the LIMK-inhibitor complexes is shown in (Supplementary Figs S10 & S11). Among the LIMK1-inhibitor complexes, the LIMK1-WPHW complex exhibited the most favorable energy contributions from conserved kinase domain residues, followed closely by the LIMK1-YFYW complex. Val366 (βIII) has contributed significantly to stabilization in complexes with LIMK1-TH470 and LIMK1-WPHW. b.l residues namely, Leu397 showed notable energy contributions in LIMK1-TH470 and LIMK1-YFYW, while Val396 contributed to LIMK1-YWFP and LIMK1-YFYW. Thr413 (GK) residue has consistently contributed to binding energy in LIMK1-TH470, LIMK1-YFYW, and LIMK1-WPHW complexes. βVII residue (Leu467) exhibited significant interaction energies in LIMK1-TH470 and LIMK1-YFYW. The XDFG Motif residues were observed to be the most predominantly contributed to the increased binding energy of the complexes; for instance, Ala477 showed favorable contributions in LIMK1-WPHW, LIMK1-YFYW, and LIMK1-YWFP. Asp478 stabilized LIMK1-WPHW and LIMK1-YFYW complexes. Meanwhile, Phe479 displayed strong energy contributions across multiple complexes, including LIMK1-TH470, LIMK1-YFYW, LIMK1-YWFP, and LIMK1-WPHW. Leu481 (a.l) significantly contributed to energy stabilization in LIMK1-TH470 and LIMK1-YWFP. Met388 (αC) residue provided favorable contributions in LIMK1-WPHW and LIMK1-YFYW complexes.

The decomposition free energy analysis reveals key contributions from conserved residues in LIMK2 that significantly influence the stability and specificity of inhibitor binding. These residues, spanning the hinge, back loop, gatekeeper, activation loop, and other conserved regions, highlight crucial interaction hotspots for ligand stabilization. The back loop residue, Leu389, demonstrated favorable interactions in LIMK2-TH470, LIMK2-FYWV, and LIMK2-WFVW complexes, highlighting its role in hydrophobic stabilization. The XDFG motif residues, particularly Ala468, contributed significantly to energy stabilization in LIMK2-TH470 and LIMK2-WFVW. Similarly, Phe470 provided stabilizing contributions in LIMK2-TH470, LIMK2-PYWG, and LIMK2-WFVW, emphasizing its importance in hydrophobic interactions. Leu472 (a.l) exhibited strong stabilizing interactions in LIMK2-TH470, LIMK2-PYWG, and LIMK2-WFVW. Leu458 (βVII) was critical in hydrophobic stabilization in LIMK2-TH470 and LIMK2-WFVW. Phe391 (βIV region) significantly stabilized binding in LIMK2-TH470, LIMK2-FYWV, and LIMK2-WFVW. Thr405 (GK) contributed notably in LIMK2-PYWG and LIMK2-WFVW, supporting ligand orientation and hinge region interactions. Lastly, Leu403 (βV) provided significant stabilizing interactions in LIMK2-FYWV and LIMK2-WFVW, reinforcing its role in hydrophobic binding.

Conclusion

Allosteric inhibitors are small molecules that bind to regions of LIMKs outside the ATP-binding site, inducing conformational changes that modulate kinase activity. These inhibitors offer significant advantages, including enhanced specificity and the ability to mitigate off-target toxicity and resistance caused by mutations in the ATP-binding pocket. A prominent example is TH470, which interacts with the DFG-out pocket and hinge region, demonstrating the potential for targeting LIMKs implicated in cancer metastasis and neurological disorders. This study prioritizes the development of tetrapeptide inhibitors that mimic the binding mode of TH470, aiming to introduce novel therapeutic strategies. Detailed analyses of LIMK1-TH470 interactions revealed critical residues, such as Thr413 (gatekeeper), Asp478 (XDFG motif), and Ile416 (hinge region), forming hydrogen bonds and hydrophobic interactions with conserved kinase residues like Lys368, Leu370, and Val476.

Similarly, LIMK2-TH470 displayed binding patterns involving Thr405 (gatekeeper), Asp469 (XDFG motif), and Ile408 (hinge region), underscoring the role of conserved residues in ensuring stable interactions. The structural features of TH470, including its 2-aminothiazole moiety as a hinge-binder and its phenylsulfamoyl moiety in the DFG-out pocket, were critical for stability. Molecular dynamics (MD) simulations of LIMK1 and LIMK2 complexes with TH470 and tetrapeptides revealed that these systems generally attained stable equilibrium, with root mean square deviations (RMSD) converging around 0.38 nm, indicating stable interactions. However, some peptide complexes, such as LIMK1-YWFP and LIMK2-FYWV, exhibited slightly higher RMSD values during simulations, suggesting reduced stability. Interaction analyses highlighted that TH470 and specific peptides (YFYW, YWFP, WPHW for LIMK1; PYWG, FYWV, WFVW for LIMK2) form stable hydrogen bonds with conserved kinase residues, particularly those in the hinge and gatekeeper regions. These interactions significantly contributed to the stability and selectivity of the complexes.

Binding free energy calculations using the MM/PBSA scheme revealed that van der Waals interactions and electrostatic energy primarily drive peptide binding. LIMK1-YFYW and LIMK2-WFVW exhibited the highest binding affinities, emphasizing their therapeutic potential. The study underscores the promise of these peptides as effective allosteric inhibitors, with stability and specificity supported by hydrophobic, electrostatic, and hydrogen bond interactions. Among the analyzed peptides, those maintaining multiple hydrogen bonds with critical LIMK residues (e.g., YFYW, YWFP for LIMK1 and PYWG, WFVW for LIMK2) demonstrated strong stability and potential for use in designing selective inhibitors targeting LIMKs. Future studies should focus on optimizing these peptides' pharmacokinetic profiles and stability in biological systems to improve their clinical potential. Expanding the application of computational and experimental methods will further refine their design and assess their efficacy across broader disease models.

Data Availability

No datasets were generated or analysed during the current study.

Supplementary information The online version contains supplementary material available at https://doi.org/10.1007/s12013-025-01718-1.

Acknowledgements JJ thanks DBT-NNP No.BT/PR40156/BTIS/137/54/2023, ST-Fund for Improvement of S &T Infrastructure in Universities Higher Educational Institutions (FIST) (SR/FST/LSI-667/2016) (C), and DST-Promotion of University Research and Scientific Excellence (PURSE phase II) (No. SR/PURSE Phase 2/38(G), 2017), MHRD-RUSA 2.0, New Delhi (F.24e51/2014-U); NH greatly acknowledges the Department of Science and Technology (DST) for financial assistance through DST/INSPIRE Fellowship/09/IF90083.

Author contributions NH: Conceptualization, Data curation, Methodology, Formal Analysis, Investigation, Visualization, Validation, Writing–original draft. SK: Investigation, Visualization, Validation, Writing–original draft; UV: Supervision, Validation, Writing–review and editing; JJ: Funding acquisition, Supervision, Validation, Writing–review and editing.

Compliance with ethical standards

Conflict of interest The authors declare no competing interests.

References

1. Cowan-Jacob, S. W., Jahnke, W., & Knapp, S. (2014). Novel approaches for targeting kinases: allosteric inhibition, allosteric activation and pseudokinases. *Future Medicinal Chemistry*, *6*, 541–561. https://doi.org/10.4155/fmc.13.216.
2. Klaeger, S., Heinzlmeir, S., Wilhelm, M., Polzer, H., Vick, B., Koenig, P. A., Reinecke, M., Ruprecht, B., Petzoldt, S., Meng, C., Zecha, J., Reiter, K., Qiao, H., Helm, D., Koch, H., Schoof, M., Canevari, G., Casale, E., Depaolini, S. R., & Feuchtinger, A. (2017). The target landscape of clinical kinase drugs. *Science*, *358*, eaan4368. https://doi.org/10.1126/science.aan4368.
3. Knapp, S. (2018). New opportunities for kinase drug repurposing and target discovery. *British Journal of Cancer*, *118*, 936–937. https://doi.org/10.1038/s41416-018-0045-6.
4. Martinez, R., Defnet, A., & Shapiro, P. (2020). Avoiding or Co-opting ATP inhibition: Overview of type III, IV, V, and VI kinase inhibitors. In P. Shapiro ed, *Next Generation Kinase Inhibitors* (pp. 29–59). Cham: Springer International Publishing.
5. Attwood, M. M., Fabbro, D., Sokolov, A. V., Knapp, S., & Schiöth, H. B. (2021). Trends in kinase drug discovery: targets, indications and inhibitor design. *Nature reviews. Drug discovery*, *20*, 839–861. https://doi.org/10.1038/s41573-021-00252-y.
6. Li, J., Gong, C., Zhou, H., Liu, J., Xia, X., Ha, W., Jiang, Y., Liu, Q., & Xiong, H. (2024). Kinase inhibitors and kinase-targeted cancer therapies: Recent advances and future perspectives. *International Journal of Molecular Sciences*, *25*, 5489. https://doi.org/10.3390/ijms25105489.
7. Goebel, G. L., Qiu, X., & Wu, P. (2022). Kinase-targeting small-molecule inhibitors and emerging bifunctional molecules. *Trends in Pharmacological Sciences*, *43*, 866–881. https://doi.org/10.1016/j.tips.2022.04.006.
8. Hanke, T., Mathea, S., Woortman, J., Salah, E., Berger, B. T., Tumber, A., Kashima, R., Hata, A., Kuster, B., Müller, S., & Knapp, S. (2022). Development and characterization of Type I, Type II, and Type III LIM-kinase chemical probes. *Journal of Medicinal Chemistry*, *65*, 13264–13287. https://doi.org/10.1021/acs.jmedchem.2c01106.
9. Goodwin, N. C., Cianchetta, G., Burgoon, H. A., Healy, J., Mabon, R., Strobel, E. D., Allen, J., Wang, S., Hamman, B. D., & Rawlins, D. B. (2015). Discovery of a Type III inhibitor of LIM kinase 2 that binds in a DFG-out conformation. *ACS Medicinal Chemistry Letters*, *6*, 53–57. https://doi.org/10.1021/ml500242y.
10. Mardilovich, K., Baugh, M., Crighton, D., Kowalczyk, D., Gabrielsen, M., Munro, J., Croft, D. R., Lourenco, F., James, D., Kalna, G., McGarry, L., Rath, O., Shanks, E., Garnett, M. J., McDermott, U., Brookfield, J., Charles, M., Hammonds, T., & Olson, M. F. (2015). LIM kinase inhibitors disrupt mitotic microtubule organization and impair tumor cell proliferation.

Oncotarget, *6*, 38469–38486. https://doi.org/10.18632/oncotarget.6288.
11. Chatterjee, D., Preuss, F., Dederer, V., Knapp, S., & Mathea, S. (2022). Structural aspects of LIMK regulation and pharmacology. *Cells*, *11*, 142. https://doi.org/10.3390/cells11010142.
12. Salah, E., Chatterjee, D., Beltrami, A., Tumber, A., Preuss, F., Canning, P., Chaikuad, A., Knaus, P., Knapp, S., Bullock, A. N., & Mathea, S. (2019). Lessons from LIMK1 enzymology and their impact on inhibitor design. *The Biochemical Journal*, *476*, 3197–3209. https://doi.org/10.1042/BCJ20190517.
13. Manetti, F. (2018). Recent advances in the rational design and development of LIM kinase inhibitors are not enough to enter clinical trials. *European Journal of Medicinal Chemistry*, *155*, 445–458. https://doi.org/10.1016/j.ejmech.2018.06.016.
14. Bernard, O. (2007). Lim kinases, regulators of actin dynamics. *The International Journal of Biochemistry & Cell Biology*, *39*, 1071–1076. https://doi.org/10.1016/j.biocel.2006.11.011.
15. Amano, T., Tanabe, K., Eto, T., Narumiya, S., & Mizuno, K. (2001). LIM-kinase 2 induces formation of stress fibres, focal adhesions and membrane blebs, dependent on its activation by Rho-associated kinase-catalysed phosphorylation at threonine-505. *The Biochemical Journal*, *354*, 149–159. https://doi.org/10.1042/0264-6021:3540149.
16. Villalonga, E., Mosrin, C., Normand, T., Girardin, C., Serrano, A., Žunar, B., Doudeau, M., Godin, F., Bénédetti, H., & Vallée, B. (2023). LIM kinases, LIMK1 and LIMK2, are crucial node actors of the cell fate: Molecular to pathological features. *Cells*, *12*, 805. https://doi.org/10.3390/cells12050805.
17. Bamburg, J. R., & Wiggan, O. P. (2002). ADF/cofilin and actin dynamics in disease. *Trends in Cell Biology*, *12*, 598–605. https://doi.org/10.1016/S0962-8924(02)02404-2.
18. Arber, S., Barbayannis, F. A., Hanser, H., Schneider, C., Stanyon, C. A., Bernard, O., & Caroni, P. (1998). Regulation of actin dynamics through phosphorylation of cofilin by LIM-kinase. *Nature*, *393*, 805–809. https://doi.org/10.1038/31729.
19. Berabez, R., Routier, S., Bénédetti, H., Plé, K., & Vallée, B. (2022). LIM kinases, promising but reluctant therapeutic targets: Chemistry and preclinical validation in vivo. *Cells*, *11*, 2090. https://doi.org/10.3390/cells11132090.
20. Kobayashi, M., Nishita, M., Mishima, T., Ohashi, K., & Mizuno, K. (2006). MAPKAPK-2-mediated LIM-kinase activation is critical for VEGF-induced actin remodeling and cell migration. *The EMBO Journal*, *25*, 713–726. https://doi.org/10.1038/sj.emboj.7600973.
21. Yoshioka, K., Foletta, V., Bernard, O., & Itoh, K. (2003). A role for LIM kinase in cancer invasion. *Proceedings of the National Academy of Sciences of the United States of America*, *100*, 7247–7252. https://doi.org/10.1073/pnas.1232344100.
22. Yamazaki, D., Kurisu, S., & Takenawa, T. (2005). Regulation of cancer cell motility through actin reorganization. *Cancer Science*, *96*, 379–386. https://doi.org/10.1111/j.1349-7006.2005.00062.x.
23. Yamaguchi, H., & Condeelis, J. (2007). Regulation of the actin cytoskeleton in cancer cell migration and invasion. *Biochimica et Biophysica Acta*, *1773*, 642–652. https://doi.org/10.1016/j.bbamcr.2006.07.001.
24. Lee-Hoeflich, S. T., Causing, C. G., Podkowa, M., Zhao, X., Wrana, J. L., & Attisano, L. (2004). Activation of LIMK1 by binding to the BMP receptor, BMPRII, regulates BMP-dependent dendritogenesis. *The EMBO Journal*, *23*, 4792–4801. https://doi.org/10.1038/sj.emboj.7600418.
25. Ohashi, K., Sampei, K., Nakagawa, M., Uchiumi, N., Amanuma, T., Aiba, S., Oikawa, M., & Mizuno, K. (2014). Damnacanthal, an effective inhibitor of LIM-kinase, inhibits cell migration and invasion. *Molecular Biology of the Cell*, *25*, 828–840. https://doi.org/10.1091/mbc.e13-09-0540.
26. Prudent, R., Vassal-Stermann, E., Nguyen, C.-H., Pillet, C., Martinez, A., Prunier, C., Barette, C., Soleilhac, E., Filhol, O., Beghin, A., Valdameri, G., Honoré, S., Aci-Sèche, S., Grierson, D., Antonipillai, J., Li, R., Di Pietro, A., Dumontet, C., Braguer, D., & Lafanechère, L. (2012). Pharmacological inhibition of LIM kinase stabilizes microtubules and inhibits neoplastic growth. *Cancer Research*, *72*, 4429–4439. https://doi.org/10.1158/0008-5472.CAN-11-3342.
27. Prunier, C., Prudent, R., Kapur, R., Sadoul, K., & Lafanechère, L. (2017). LIM kinases: cofilin and beyond. *Oncotarget*, *8*, 41749–41763. https://doi.org/10.18632/oncotarget.16978.
28. Sleebs, B. E., Nikolakopoulos, G., Street, I. P., Falk, H., & Baell, J. B. (2011). Identification of 5,6-substituted 4-aminothieno2,3-dpyrimidines as LIMK1 inhibitors. *Bioorganic & Medicinal Chemistry Letters*, *21*, 5992–5994. https://doi.org/10.1016/j.bmcl.2011.07.050.
29. Vadevoo, S. M. P., Gurung, S., Lee, H.-S., Gunassekaran, G. R., Lee, S. M., Yoon, J. W., Lee, Y. K., & Lee, B. (2023). Peptides as multifunctional players in cancer therapy. *Experimental & Molecular Medicine*, *55*, 1099–1109. https://doi.org/10.1038/s12276-023-01016-x.
30. Wang, L., Wang, N., Zhang, W., Cheng, X., Yan, Z., Shao, G., Wang, X., Wang, R., & Fu, C. (2022). Therapeutic peptides: current applications and future directions. *Signal Transduction and Targeted Therapy*, *7*, 48. https://doi.org/10.1038/s41392-022-00904-4.
31. Bogoyevitch, M. A., Barr, R. K., & Ketterman, A. J. (2005). Peptide inhibitors of protein kinases-discovery, characterisation and use. *Biochimica et Biophysica Acta*, *1754*, 79–99. https://doi.org/10.1016/j.bbapap.2005.07.025.
32. Bharathikumar, V. M., Barreto, K., Decoteau, J. F., & Geyer, C. R. (2013). Allosteric lariat peptide inhibitors of Abl kinase. *Chembiochem*, *14*, 2119–2125. https://doi.org/10.1002/cbic.201300253.
33. Biswas, B., Huang, Y.-H., Craik, D. J., & Wang, C. K. (2024). The prospect of substrate-based kinase inhibitors to improve target selectivity and overcome drug resistance. *Chemical Science*, *15*, 13130–13147. https://doi.org/10.1039/D4SC01088D.
34. Boohaker, R. J., Lee, M. W., Vishnubhotla, P., Perez, J. M., & Khaled, A. R. (2012). The use of therapeutic peptides to target and to kill cancer cells. *Current Medicinal Chemistry*, *19*, 3794–3804. https://doi.org/10.2174/092986712801661004.
35. Ciulla, M. G., Civera, M., Sattin, S., Kumar, K. (2023). Nature-inspired and medicinally relevant short peptides. *Exploration of Drug Science*, 140–171. https://doi.org/10.37349/eds.2023.00011.
36. Naeimi, R., Bahmani, A., & Afshar, S. (2022). Investigating the role of peptides in effective therapies against cancer. *Cancer Cell International*, *22*, 139 https://doi.org/10.1186/s12935-022-02553-7.
37. Lee, H., Yosaatmadja, Y., Burgess-Brown, N. A., von Delft, F., Arrowsmith, C. H., Edwards, A., Bountra, C., Elkins, J. M. (2022). Structure of LIMK1 kinase domain with allosteric inhibitor TH-470.
38. Mathea, S., Salah, E., Hanke, T., & Knapp, S. (2021). LIM domain kinase 2 (LIMK2) in complex with TH-470.
39. Eswar, N., Webb, B., Marti-Renom, M. A., Madhusudhan, M. S., Eramian, D., Shen, M. Y., Pieper, U., & Sali, A. (2006). Chapter 5, 5 Comparative protein structure modeling using Modeller. *Current Protocols in Bioinformatics*, *Chapter 5*, Unit-5.6. https://doi.org/10.1002/0471250953.bi0506s15.
40. Kumar, A., Rajendran, V., Sethumadhavan, R., & Purohit, R. (2014). Relationship between a point mutation S97C in CK1δ protein and its affect on ATP-binding affinity. *Journal of Biomolecular Structure & Dynamics*, *32*, 394–405. https://doi.org/10.1080/07391102.2013.770373.
41. Eberhardt, J., Santos-Martins, D., Tillack, A. F., & Forli, S. (2021). AutoDock Vina 1.2.0: New Docking Methods, Expanded Force Field, and Python Bindings. *Journal of Chemical*

Information And Modeling, *61*, 3891–3898. https://doi.org/10.1021/acs.jcim.1c00203.
42. Bauer, P., Hess, B., Lindahl, E. (2022). GROMACS 2022.1 Manual. https://doi.org/10.5281/zenodo.6451567.
43. Ansar, S., & Vetrivel, U. (2019). PepVis: An integrated peptide virtual screening pipeline for ensemble and flexible docking protocols. *Chemical Biology & Drug Design*, *94*, 2041–2050. https://doi.org/10.1111/cbdd.13607.
44. Rodrigues, C. H. M., Garg, A., Keizer, D., Pires, D., & Ascher, D. B. (2022). CSM-peptides: A computational approach to rapid identification of therapeutic peptides. *Protein Science*, *31*, e4442. https://doi.org/10.1002/pro.4442.
45. Wei, L., Ye, X., Sakurai, T., Mu, Z., & Wei, L. (2022). ToxIBTL: prediction of peptide toxicity based on information bottleneck and transfer learning. *Bioinformatics*, *38*, 1514–1524. https://doi.org/10.1093/bioinformatics/btac006.
46. Rathore, A. S., Choudhury, S., Arora, A., Tijare, P., & Raghava, G. (2024). ToxinPred 3.0: An improved method for predicting the toxicity of peptides. *Computers in Biology and Medicine*, *179*, 108926. https://doi.org/10.1016/j.compbiomed.2024.108926.
47. Salentin, S., Schreiber, S., Haupt, V. J., Adasme, M. F., & Schroeder, M. (2015). PLIP: fully automated protein-ligand interaction profiler. *Nucleic Acids Research*, *43*, W443–W447. https://doi.org/10.1093/nar/gkv315.
48. Weng, G., Wang, E., Wang, Z., Liu, H., Zhu, F., Li, D., & Hou, T. (2019). HawkDock: a web server to predict and analyze the protein-protein complex based on computational docking and MM/GBSA. *Nucleic Acids Research*, *47*, W322–W330. https://doi.org/10.1093/nar/gkz397.
49. Valdés-Tresanco, M. S., Valdés-Tresanco, M. E., Valiente, P. A., & Moreno, E. (2021). gmx_MMPBSA: A new tool to perform end-state free energy calculations with GROMACS. *Journal of Chemical Theory And Computation*, *17*, 6281–6291. https://doi.org/10.1021/acs.jctc.1c00645.
50. Sharma, B., Bhattacherjee, D., Zyryanov, G. V., & Purohit, R. (2023). An insight from computational approach to explore novel, high-affinity phosphodiesterase 10A inhibitors for neurological disorders. *Journal of Biomolecular Structure & Dynamics*, *41*, 9424–9436. https://doi.org/10.1080/07391102.2022.2141895.
51. Singh, R., & Purohit, R. (2023). Computational analysis of protein-ligand interaction by targeting a cell cycle restrainer. *Computer Methods and Programs in Biomedicine*, *231*, 107367. https://doi.org/10.1016/j.cmpb.2023.107367.
52. Bhardwaj, V., Singh, R., Singh, P., Purohit, R., & Kumar, S. (2020). Elimination of bitter-off taste of stevioside through structure modification and computational interventions. *Journal of Theoretical Biology*, *486*, 110094. https://doi.org/10.1016/j.jtbi.2019.110094.